

Plasmonic structure integrated superconducting nanowire single-photon detector with BSCCO stripes

András Szenes^{1,2}, László Pothorcki^{1,2}, Balázs Bánhelyi^{2,3}, and Mária Csete^{1,2,*}

1. *Department of Optics and Quantum Electronics, University of Szeged, 6720, Dóm tér 9, Szeged, Hungary.*

2. *HUN-REN Wigner Research Center of Physics, Konkoly-Thege Miklós út 29-33, Budapest, Hungary.*

3. *the Department of Computational Optimization, University of Szeged, 6720, Árpád tér 2, Szeged.*

* *mcsete@physx.u-szeged.hu*

ABSTRACT Superconducting nanowire single-photon detectors (SNSPDs) were integrated with plasmonic nanostructures to enhance the absorption efficiency of superconducting BSCCO stripes. A numerical investigation of optimized nanocavity array (NCAI) and nanocavity-trench-array (NCTAI) SNSPDs has revealed that more than one order of magnitude larger absorptance can be achieved at perpendicular incidence, when compared to the corresponding meandered BSCCO pattern in a resonant optical cavity. The SNSPDs were considerably improved either via first and third quarter cavity resonances, as evidenced by the near-field maps and validated by the standard retrieval method. Although, NCAI-SNSPD exhibits slightly larger absorptance, NCTAI-SNSPD remains competitive due to its larger period and significantly smaller filling factor, thereby allowing for quicker electric response.

KEYWORDS - single-photon detector, numerical optimization, plasmonics, nanocavity, cuprate

I. INTRODUCTION

The detection of single-photons encompasses numerous fields of fundamental research and applications, notably in the secure information transfer and has potential role in quantum computing and quantum communication [1], [2], [4]. Among single-photon detectors, superconducting nanowire single-photon detectors (SNSPDs) have remarkable properties [3]. These detectors operate based on the modification of the superconducting state in the nanowires constituting their absorbing segments, as the single-photon induced hot spot is capable of breaking the superconducting equilibrium. The consequent increase beyond the critical current manifests itself in a voltage jump in the readout electronics [5]. Exploiting this phenomenon, SNSPDs offer operation across a wide range of wavelengths (from X-ray to mid-IR) and enable high efficiency as well as picosecond time-resolution [6], [7], [8], [9]. However, a drawback of SNSPDs is their basis on superconductivity, restricting their operation to very low temperatures, typically below 4.2 K, in the case of e.g. niobium-nitride (NbN) superconductors. This cryogenic temperature requirement constrains their wide-range applicability and made them expensive.

Efforts have been made to develop high-critical-temperature cuprate superconductors for SNSPDs, yet experimentally detecting single-photons above 4.2 K was not successful [10], [11]. The primary challenge lies in the manufacturing difficulties, as the traditional SNSPD fabrication procedures severely damage cuprate superconductors. Recently, a method has been developed, whereby non-superconducting patterns are drawn into helium-ion-exposed Bi₂Sr₂CaCu₂O_{8+δ} (BSCCO) flakes encapsulated into hBN, thus achieving desired patterns without damaging the material. With this method, with BSCCO superconductors good single-photon sensitivity has been demonstrated at telecommunication wavelengths (1550 nm), even up until temperatures of 20-25 K [12], [13]. Thus-formed novel generation SNSPDs can be operable with simpler cooling systems, even in larger-scale patterns.

The next challenge is enhancing the absorption efficiency of the nanowire pattern. One of the previously demonstrated approaches is placing the superconducting nanowires into an optical cavity [14], [15]. Our previous studies have shown that in addition to optical cavities, significant improvements can be achieved by integrating periodic nanoplasmonic patterns [16], [17], [18], [19]. Integration of plasmonic patterns enables the application of relatively high (wavelength-scaled) periodicity nanowire patterns in a wide wavelength-range and within a specific range of incidence angles, while maintaining high efficiency (>90%) [20], [21], [22]. The large period reduces the kinetic inductance of the nanowire pattern, thus increasing the speed of the detector [23].

In this study, the numerical optimization of BSCCO-based SNSPDs integrated with plasmonic patterns was performed to maximize the absorption in the nanowires, thereby determining the optimal geometry for efficient operation at telecommunication wavelengths. The higher operational temperature makes these SNSPDs suitable for integrated photonic circuits, and high efficiency SNSPDs operable as integrated on-chip optical components pave the way for new quantum optical applications .,

II. METHODS

The geometries of SNSPDs were designed in a numerical environment, with the RF module of FEM-based COMSOL Multiphysics software package, by solving the full-wave Maxwell equations, considering the material's dispersion by importing tabulated datasets [24], [25]. The optical response of different device compositions, specifically absorption (arising as a loss from resistive heating in materials with non-zero imaginary parts of their permittivity), reflection, and transmission (computed as the outgoing power density integrated on ports in the forward and backward directions), was determined as a function of wavelength and angle of incidence, by using single unit cells of the inspected periodic patterns terminated by Floquet boundary conditions.

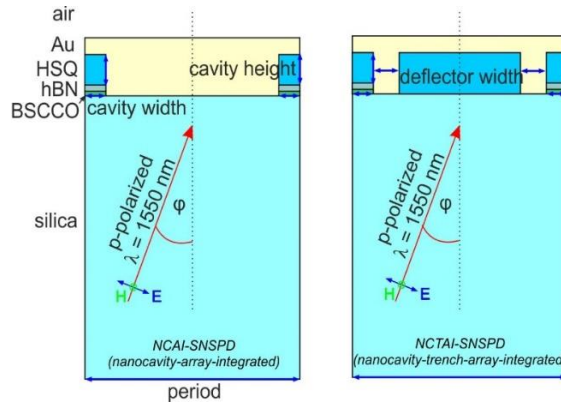


Fig. 1. Schematic of the unit cells of the inspected NCAI-SNSPD and NCTAI-SNSPD periodic structures, indicating the illumination by p-polarized light and the parameters varied during optimization.

The superconducting material segment was a 15 nm thick BSCCO layer covered by a 20 nm hBN film, defined by their full permittivity tensor accounting for the thin films bianisotropy [26], [27] (Figure S1 in Supplementary Material). The optimization of the geometry was realized to maximize the amount of power absorbed in the BSCCO wires. The optimization was performed at the wavelength of 1550 nm, important for telecommunication applications, and normal incidence was supposed during the optimization performed by using p-polarized light in S-configuration [20].

During this study two types of integrated SNSPD device compositions were inspected (Figure 1). In both compositions the 15 nm thick meandered BSCCO wire is positioned onto a silica substrate and covered by the 20 nm hBN and an HSQ layer, with a thickness varied in the [10 nm, 800 nm] interval during optimization. On the top of the HSQ layer a fixed 60 nm thick gold reflector closes an optical cavity that is filled with HSQ. In the first inspected device composition the wires were separated by bulk gold segments laterally, forming a nanocavity-array (NCAI – nanocavity-array-integrated SNSPD), with a wire-to-wire distance that was varied in the [800 nm, 1200 nm] interval. In the second device composition the width of the lateral walls of the cavities was also varied, thereby allowing for “opening an empty trench array”. The BSCCO&hBN filled cavities and the empty trenches create a nanocavity-trench-array (NCTAI – nanocavity-trench-array-integrated SNSPD). Both inspected composition types are inherited from the integrated devices optimized in our previous studies to improve SNSPD absorption, when it was shown that by introducing a secondary nanocavity (trench) array, even greater absorptance can be achieved, due to the minimized competitive gold absorption [20], [21], [22]. The geometrical parameters of both compositions were optimized using COMSOL Multiphysics Optimization Module and an in-house developed GLOBAL algorithm [28].

During the first part of optimization, a Monte Carlo searching was conducted to determine the period, cavity height, (deflector width) and wire width in NCAI (NCTAI) SNSPD, with a potential to maximize the achievable absorptance. As the second step a local search was performed to find the global maxima in the inspected geometrical parameter region of interest.

In this study NCAI-SNSPD and NCTAI-SNSPD compositions were numerically optimized at 1550 nm operation wavelength, illuminated at normal-incidence in p-to-S configuration, with an objective function to maximize BSCCO absorptance [20]. The far-field and near-field responses of the optimized device compositions were thoroughly investigated to uncover the underlying physics. The dispersion characteristics of the two integrated device compositions taken in p-to-S configuration were compared to each other and to those of simple optical cavities, in order to characterize their potential in fast single-photon counting devices at 1550 nm.

III. RESULTS AND DISCUSSION

A. Reference configurations

To define a reference for our optimized nanostructure-integrated SNSPDs, compositions involving (i) a continuous BSCCO slab (Figure S2), (ii) covered with an optical cavity (Figure S3), and (iii) a meandered BSCCO pattern within an optical cavity (Figure S4) were first investigated.

In the case of a continuous slab, 15.1% BSCCO absorptance is achieved at 1550 nm at perpendicular incidence, which is accompanied by 84.2% transmittance (Figure S2). The absorptance can be further increased by extending the operation wavelength region (17.0% at 1750 nm), which is due to the increasing imaginary part of BSCCO permittivity. Oblique incidence is also advantageous in this composition, as it is demonstrated by reaching 20.3% absorptance at 59° angle of incidence, which is due to the propagating mode on the BSCCO slab.

The optical cavity (OC) is formed by placing a 60 nm gold reflector above the BSCCO slab (Figure S3). To maximize absorptance, the cavity length is tuned to 225 nm. At 1550 nm and at perpendicular incidence, 39.4% absorptance is achieved, which is accompanied by zero transmittance, a minimal competitive Au absorptance, and a high reflectivity. The absorptance can be further increased by extending the operation wavelength region (42.1% at 1750 nm); however, tilting is not advantageous in this composition.

To ensure better comparability with our optimized nano-cavity-array compositions, a meandered pattern of BSCCO is inserted instead the continuous BSCCO slab, while the optical cavity remains unchanged (Figure S4). In this case, the BSCCO absorptance drops to 7.0% at 1550 nm at perpendicular incidence, which is caused by the low fill-factor of the absorbing material. The absorptance can be further increased to 8.5% by extending the wavelength region to 1750 nm. The decrease in absorptance is 0.18-fold (Table S1) compared to the continuous slab, which is not as large as expected from the 0.1-fold decrease in filling factor. By increasing the tilting, the BSCCO absorptance monotonously decreases in the meandered stripes. It originates from the gradually modifying reflection coefficient, and that the device composition is optimized for perpendicular incidence.

B. Nanocavity array

Dividing the optical cavity with vertical gold segments creates a nanocavity array, which is the common element of the proposed plasmonic structure integrated SNSPDs (Figure 1).

According to the initial Monte Carlo simulations in both the nanocavity-array-integrated (NCAI-SNSPD) and the nanocavity-trench-array-integrated (NCTAI-SNSPD) compositions, two absorptance peaks emerge as a function of cavity height, that correspond to the $\lambda/4$ and $3\times\lambda/4$ modes of the nanocavities (Figure S5 and S6).

In the case of NCAI-SNSPD, absorptance plateaus were observed for larger cavity widths and smaller periods (i.e., corresponding to increasing filling factor, Figure S5). The result of plateauing is that a significant reduction in period or increase in wire width is not accompanied by a significant decrease in absorption. A trade-off exists for this composition, therefore using a larger period, allowing for a reduction in kinetic inductance and thus an increase in detector speed, with only a small compromised decrease in absorption, is reasonable to consider.

In the case of NCTAI-SNSPD, a global maximum was observed as a function of cavity width, period and deflector width at smaller /intermediate /larger values, respectively. This predicts the existence of a global optimum (Figure S6).

Following the Monte Carlo simulations, local searches were realized with NCAI-SNSPD and NCTAI-SNSPD around the two absorptance peaks corresponding to different cavity modes (Figure 2 and 3).

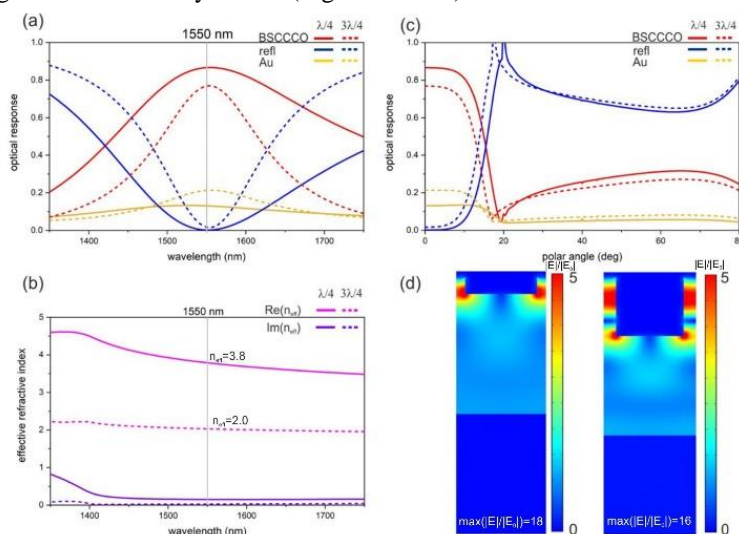


Fig. 2. Optical response of optimized NCAI-SNSPD composition in p-to-S configuration. (a) spectrum and (b) polar angle dependence. Solid: mode 1 (smaller cavity height) dashed: mode 2 (larger cavity height). Time averaged near-field enhancement of NCAI-SNSPD optimized to resonate in the (c) mode 1 and (d) mode 2.

The NCAI-SNSPD optimized to resonate in the $\lambda/4$ cavity mode exhibits a broad Lorentzian-resonance in absorptance centered around 1550 nm (Figure 2a solid lines). The peak absorptance of NCAI-SNSPD is 86.6%, which is accompanied by a negligible reflectance and transmittance, and 13.1% competitive gold absorptance. The BSCCO absorptance reaches a global maximum at perpendicular incidence, as indicated by the polar angle-dependent optical response, at the center of a pass band (Figure 2b solid lines). In the close vicinity of the BSCCO nanowire 18-fold near-field enhancement is observable (Figure 2c).

When optimized for the cavity mode resonating in a nanocavity of $3\times\lambda/4$ length, the NCAI-SNSPD shows a smaller and narrower absorptance peak centered around 1550 nm (Figure 2a dashed lines). The higher Q-factor is typical for higher-order plasmonic resonances. The maximal absorptance is 75.9%, accompanied by a small, but not negligible reflectance and a higher gold absorptance (21.4%), when compared to those achieved in NCAI-SNSPD optimized for resonance in the $\lambda/4$ cavity mode. The polar angle dependence of the optical responses in case of the higher-order mode closely resembles that monitored in case of the $\lambda/4$ cavity mode, with consistently smaller absorptance values and extrema occurring at slightly smaller polar angles (Figure 2b dashed lines). The highest absorptance is achieved at perpendicular incidence, similarly at the center of a slightly narrower pass-band. A 16-fold near-field enhancement is observable, which is slightly smaller compared to NCAI-SNSPD optimized to resonate in the $\lambda/4$ cavity mode (Figure 2d).

Standard retrieval calculations [29] indicate that the calculated cavity lengths correspond to approximately $\lambda/(4 \times n_{\text{eff}})$ and $3 \times \lambda/(4 \times n_{\text{eff}})$ with good precision (Figure 2a solid and dashed wine lines).

The NCTAI-SNSPD is optimized similarly to resonate in the $\lambda/4$ and $3 \times \lambda/4$ modes (Figure 3). In case of the lower order mode the absorption spectrum of the optimized NCTAI-SNSPD reveals an inverted minigap in absorptance, which is extended towards larger wavelengths, with its peak appearing at 1550 nm (Figure 3a solid lines). At smaller wavelengths, the absorptance monotonically and rapidly decreases, except for a small local maximum corresponding to a secondary counter-propagating coupled mode. The global maximum in the absorptance spectrum is 83.3%, which is accompanied by a negligible reflectance and transmittance, and a relatively large competitive gold absorptance (16.5%). This maximum is attained at perpendicular incidence (Figure 3b solid lines). At larger polar angles, the absorptance rapidly decreases, while at intermediate values, it exhibits a wider, shallower local absorptance maximum. At the global maximum a 25-fold near-field enhancement is observable (Figure 3c).

When optimized to resonate in the $3 \times \lambda/4$ mode, the NCTAI-SNSPD displays a significantly narrower peak in the absorptance spectrum, which is precisely centered at 1550 nm (Figure 3a dashed lines). The absorptance rapidly decreases below and above 1550 nm. The maximal absorptance is 65.9%, accompanied by a small reflectance and a more significant competitive gold absorptance (32.8%). This maximum is reached at perpendicular incidence, with the absorptance more rapidly decreasing at small tilting, while a small local maximum appears at slightly larger polar angles (Figure 3b dashed lines). The near-field enhancement at the global maximum is 19-fold, which is slightly smaller compared to NCTAI-SNSPD optimized to resonate in the $\lambda/4$ cavity mode (Figure 3d).

Standard retrieval for perpendicular incidence reveals that the optimized nanocavity structure has an effective refractive index, which results in $\lambda/4 \times n_{\text{eff}}$ and $3 \times \lambda/4 \times n_{\text{eff}}$ at the first and third nanocavity resonance (Figure 3a solid and dashed wine lines).

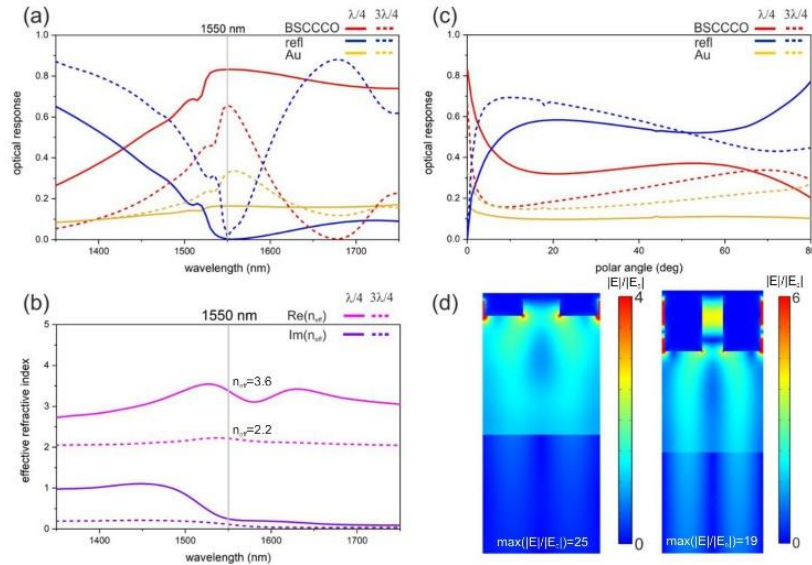


Fig. 3. Optical response of optimized NCTAI-SNSPD composition in p-to-S configuration. (a) spectrum and (b) polar angle dependence. Solid: mode 1 (smaller cavity height) dashed: mode 2 (larger cavity height). Time-averaged near-field enhancement of NCTAI-SNSPD optimized to resonate in the (c) mode 1 and (d) mode 2.

C. Comparative study

The absorptance spectrum and polar angle dependence of NCAI-SNSPD and NCTAI-SNSPD reveal distinct resonant modes in the optimized integrated plasmonic gratings. To analyze the underlying physics, the dispersion diagrams of the optimized composition in p-to-S configuration is calculated (Figure 4). The optimal NCAI-SNSPD composition exhibits well-defined low energy plasmonic mode below the first order grating coupling (Figure 4a and 4b). The branches are folded back into the first Brillouin zone and result in a single Lorentzian-shaped resonance in the wavelength dependence at perpendicular incidence (Figure 2a). The absorptance remains large over a relatively wide polar angle interval (at incidence angles of 16.5° and 14.6° , the absorption decreases to $1/e$ of its maximum value for the NCAI and NCTAI, respectively.) but sharply decreases below 5° around 20° tilting, which is in accordance with that the edge of this pass band is tuned to 1550 nm. Along the grating-coupled branches the absorptance of BSCCO is diminished, however at large tilting the absorptance is enhanced in a wide polar angle and wavelength interval across the second Brillouin zone. This correspond to the plasmonic Brewster angle (PBA), its condition is met, when the grating is impedance matched with the substrate and results in anomalous energy squeezing into and tunneling through the cavity-array, hence suppressed reflection and enhanced absorption [30], [31]. The maximum of PBA region is centered below 1550 nm. It can be noted, that both the propagating plasmonic resonance and the PBA related peaks are much narrower in frequency in the optimized composition with $3 \times \lambda/4$ cavity length, which indicate modes of longer lifetime. This is also confirmed by eigenmode calculations which results in $\omega_{\text{NCAI}, \lambda/4} = (1.24 + 0.14i) \times 10^{15}$ 1/s and $\omega_{\text{NCAI}, 3 \times \lambda/4} = (1.21 + 0.07i) \times 10^{15}$ 1/s, 1523 nm and 1556 nm respectively) [32].

The optimal NCTAI compositions display multiple peaks around 1550 nm, which reveals the co-existence of coupled modes. The propagating plasmonic mode folded back to the first Brillouin zone due to that the first order grating coupled branch is observable in NCTAI-SNSPD as well, however it is tuned to smaller frequency ($\omega_{\text{NCTAI}_{1 \times \lambda/4}} = (0.99+0.05i) \times 10^{15} \text{ 1/s}$ and $\omega_{\text{NCTAI}_{3 \times \lambda/4}} = (1.10+0.07i) \times 10^{15} \text{ 1/s}$).

What makes NCTAI-SNSPD even more different from NCAI-SNSPD compositions is that grating-coupling into surface modes appearing along tilted branches enhances the absorptance of BSCCO at small polar angles. In the dispersion diagram of optimized NCTAI-SNSPD compositions an inverted minigap emerges at the crossing of first order forward and backward propagating coupled modes, whose lower edge is tuned exactly to 1550 nm. The PBA appears in NCTAI-SNSPD as well, although the related absorption peak is much narrower and appears also at smaller frequencies due to the larger BSCCO period. The longer cavities result in narrower resonances, as they support plasmonic resonances of higher order mode and Q-factor .

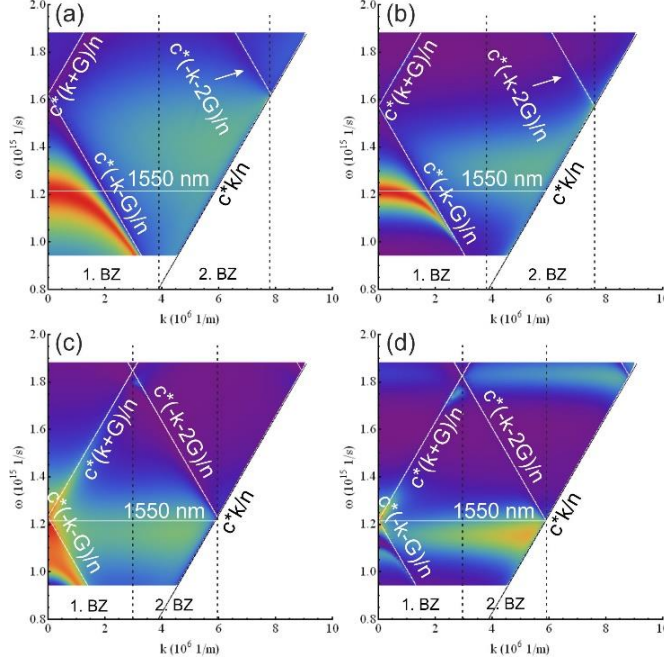


Fig. 4. Dispersion diagram in absorption of (a) NCAI-SNSPD in mode 1, (b) NCAI-SNSPD in mode 2, (c) NCTAI-SNSPD in mode 1 and (d) NCTAI-SNSPD in mode 2

Comparing the optimized integrated devices, the NCAI-SNSPD exhibits larger BSCCO absorptance and smaller Au absorptance than the NCTAI-SNSPD (despite the trench array). The difference is 3.3% and 10% for $\lambda/4$ mode and $3 \times \lambda/4$ mode, respectively. However, it's important to note that in NCTAI-SNSPD, these absorptance values are achieved with a pattern of significantly larger period (which is preferable for faster operation due to the related smaller kinetic inductance) despite a smaller cavity width, i.e., a smaller volume fill-factor. Thus, NCTAI-SNSPD emerges as a competitive geometry due to the insertion of a secondary trench cavity array. Contrary to the relations regarding the absorptance in BSCCO, the near-field enhancement correlates with the absorptance in gold, hence it is larger in NCTAI-SNSPD configurations for both inspected nanocavity resonant mode orders.

V. CONCLUSION

In conclusion, the plasmonic grating integrated SNSPD based on BSCCO nanowire pattern is optimized to maximize absorptance at 1550 nm and perpendicular incidence. The nanocavity array optical responses proves the capability to increase absorptance by more than an order of magnitude compared to a simple optimized optical cavity and an embedded meandered BSCCO pattern with a similar 0.1 filling factor. Both the $\lambda/4$ and $3 \times \lambda/4$ scaled nanocavity arrays are capable of maximizing absorptance, but the lower order cavity resonance in shorter cavity consistently results in larger BSCCO absorptance with smaller competitive gold absorptance and reflectance.

While the NCAI-SNSPD possesses larger BSCCO absorptance, it is achieved with a larger filling factor compared to NCTAI-SNSPD, which is competitive in the electrical response time.

ACKNOWLEDGEMENT

This work has been supported by the National Research, Development and Innovation Office (NKFIH) of Hungary, via the projects: “Optimized nanoplasmonics” (K116362), “Nanoplasmonic Laser Inertial Fusion Research Laboratory” (2022-2.1.1-NL-2022-00002 and 2020-2.1.1-ED-2024-00314) and “National Laboratory for Cooperative Technologies” (NKFIH-2022-2.1.1-NL-2022-00012) in the framework of the Hungarian National Laboratory program.

REFERENCES

- [1] E. Knill, R. Laflamme, and G. J. Milburn, “A scheme for efficient quantum computation with linear optics,” *Nature*, vol. 409, no. 6816, pp. 46–52, Jan. 2001, doi: 10.1038/35051009.
- [2] H. Wang *et al.*, “High-efficiency multiphoton boson sampling,” *Nat. Photonics*, vol. 11, no. 6, pp. 361–365, Jun. 2017, doi: 10.1038/nphoton.2017.63.
- [3] R. H. Hadfield, “Single-photon detectors for optical quantum information applications,” *Nat. Photonics*, vol. 3, no. 12, pp. 696–705, Dec. 2009, doi: 10.1038/nphoton.2009.230.
- [4] S. -K. Liao *et al.*, “Satellite-relayed intercontinental quantum network,” *Phys. Rev. Lett.*, vol. 120, no. 3, Jan. 2018, Art. no. 030501, doi: 10.1103/PhysRevLett.120.030501.
- [5] C. M. Natarajan, M. G. Tanner, and R. H. Hadfield, “Superconducting nanowire single-photon detectors: physics and applications,” *Supercond. Sci. Technol.*, vol. 25, no. 6, Apr. 2012, Art. no. 063001, doi: 10.1088/0953-2048/25/6/063001.
- [6] M. A. Wolff *et al.*, “Broadband waveguide-integrated superconducting single-photon detectors with high system detection efficiency,” *Appl. Phys. Lett.*, vol. 118, no. 15, Apr. 2021, Art. no. 154004, doi: 10.1063/5.0046057.
- [7] D. V. Reddy, R. R. Nerem, S. W. Nam, R. P. Mirin, and V. B. Verma, “Superconducting nanowire single-photon detectors with 98% system detection efficiency at 1550 nm,” *Optica*, vol. 7, no. 12, pp. 1649–1653, Dec. 2020, doi: 10.1364/OPTICA.400751.
- [8] J. Chang *et al.*, “Detecting telecom single photons with 99.5% system detection efficiency and high time resolution,” *APL Photonics*, vol. 6, no. 3, Mar. 2021, Art. no. 036114, doi: 10.1063/5.0039772.
- [9] I. Esmail Zadeh *et al.*, “Superconducting nanowire single-photon detectors: A perspective on evolution, state-of-the-art, future developments, and applications,” *Appl. Phys. Lett.*, vol. 118, no. 19, May 2021, Art. no. 190502, doi: 10.1063/5.0045990.
- [10] M. Ejmaes *et al.*, “Observation of dark pulses in 10 nm thick YBCO nanostrips presenting hysteretic current voltage characteristics,” *Supercond. Sci. Technol.*, vol. 30, no. 12, Nov. 2017, Art. no. 12LT02, doi: 10.1088/1361-6668/aa94b9.
- [11] E. Andersson, R. Arpaia, E. Trabaldo, T. Bauch, and F. Lombardi, “Fabrication and electrical transport characterization of high quality underdoped YBa₂Cu₃O_{7- δ} nanowires,” *Supercond. Sci. Technol.*, vol. 33, no. 6, Apr. 2020, Art. no. 064002, doi: 10.1088/1361-6668/ab807e.
- [12] I. Charaev *et al.*, “Single-photon detection using high-temperature superconductors,” *Nat. Nanotechnol.*, vol. 18, no. 4, pp. 343–349, Apr. 2023, doi: 10.1038/s41565-023-01325-2.
- [13] R. L. Merino *et al.*, “Two-dimensional cuprate nanodetector with single telecom photon sensitivity at T = 20 K,” *2D Mater.*, vol. 10, no. 2, Feb. 2023, Art. no. 021001, doi: 10.1088/2053-1583/acb4a8.
- [14] S. Miki, M. Takeda, M. Fujiwara, M. Sasaki, and Z. Wang, “Compactly packaged superconducting nanowire single-photon detector with an optical cavity for multichannel system,” *Opt. Express*, vol. 17, no. 26, pp. 23557–23564, Dec. 2009, doi: 10.1364/OE.17.023557.
- [15] F. Marsili *et al.*, “Detecting single infrared photons with 93% system efficiency,” *Nat. Photonics*, vol. 7, no. 3, pp. 210–214, Mar. 2013, doi: 10.1038/nphoton.2013.13.
- [16] M. Csete, A. Sipos, F. Najafi, X. Hu, and K. K. Berggren, “Numerical method to optimize the polar-azimuthal orientation of infrared superconducting nanowire single-photon detectors,” *Appl. Opt.*, vol. 50, no. 31, pp. 5949–5956, Nov. 2011, doi: 10.1364/AO.50.005949.
- [17] M. Csete, Á. Sipos, F. Najafi, and K. K. Berggren, “Optimized polar-azimuthal orientations for polarized light illumination of different superconducting nanowire single-photon detector designs,” *J. Nanophotonics*, vol. 6, no. 1, Nov. 2012, Art. no. 063523, doi: 10.1117/1.JNP.6.063523.
- [18] M. Csete, A. Szalai, Á. Sipos, and G. Szabó, “Impact of polar-azimuthal illumination angles on efficiency of nano-cavity-array integrated single-photon detectors,” *Opt. Express*, vol. 20, no. 15, pp. 17065–17081, Jul. 2012, doi: 10.1364/OE.20.017065.
- [19] M. Csete, Á. Sipos, A. Szalai, F. Najafi, G. Szabó, and K. K. Berggren, “Improvement of infrared single-photon detectors absorptance by integrated plasmonic structures,” *Sci. Rep.*, vol. 3, no. 1, Aug. 2013, Art. no. 2406, doi: 10.1038/srep02406.
- [20] M. Csete, G. Szekeres, A. Szenes, A. Szalai, and G. Szabó, “Plasmonic Structure Integrated Single-Photon Detector Configurations to Improve Absorptance and Polarization Contrast,” *Sensors*, Feb. 2015, vol. 15, no. 2, pp. 3513–3539, doi: 10.3390/s150203513.
- [21] M. Csete, G. Szekeres, A. Szenes, B. Bánhelyi, T. Csendes, and G. Szabo, “Optimized Superconducting Nanowire Single Photon Detectors to Maximize Absorptance,” *Prog. Electromagn. Res. B*, vol. 65, pp. 81–108, Jan. 2016, doi: 10.2528/PIERB15090904.
- [22] B. Tóth, A. Szenes, D. Marácz, B. Bánhelyi, T. Csendes, and M. Csete, “Polarization Independent High Absorption Efficiency Single-Photon Detectors Based on Three-Dimensional Integrated Superconducting And Plasmonic Patterns,” *IEEE J. Sel. Top. Quantum Electron.*, vol. 26, no. 3, May-Jun. 2020, Art. no. 3900309, doi: 10.1109/JSTQE.2020.2987131.
- [23] A. J. Kerman *et al.*, “Kinetic-inductance-limited reset time of superconducting nanowire photon counters,” *Appl. Phys. Lett.*, vol. 88, no. 11, Mar. 2006, Art. no. 111116, doi: 10.1063/1.2183810.
- [24] P. B. Johnson and R. W. Christy, “Optical Constants of the Noble Metals,” *Phys. Rev. B*, vol. 6, no. 12, pp. 4370–4379, Dec. 1972, doi: 10.1103/PhysRevB.6.4370.
- [25] I. H. Malitson, “Interspecimen comparison of the refractive index of fused silica,” *J. Opt. Soc. Am.*, vol. 55, no. 10, pp. 1205–1209, Oct. 1965, doi: 10.1364/JOSA.55.001205.
- [26] M. B. Romanowsky and F. Capasso, “Orientation-dependent Casimir force arising from highly anisotropic crystals: Application to Bi₂Sr₂CaCu₂O_{8+ δ} ,” *Phys. Rev. A*, vol. 78, no. 4, Oct. 2008, Art. no. 042110, doi: 10.1103/PhysRevA.78.042110.
- [27] Z. Yuan, R. Che, P. Li, A. Y. Nikitin, R. Hillenbrand, and X. Zhang, “Extremely Confined Acoustic Phonon Polaritons in Monolayer-hBN/Metal Heterostructures for Strong Light–Matter Interactions,” *ACS Photonics*, Sep. 2020, vol. 7, no. 9, pp. 2610–2617, doi: 10.1021/acsp Photonics.0c00981.
- [28] T. Csendes, L. Pál, J. O. H. Sendin, and J. R. Banga, “The GLOBAL optimization method revisited,” *Optim Lett*, Nov. 2007, vol. 2, pp. 445–454, doi: 10.1007/s11590-007-0072-3.
- [29] Z. Szabó, G. -H. Park, R. Hedge, and E. -P. Li, “A Unique Extraction of Metamaterial Parameters Based on Kramers–Kronig Relationship,” *IEEE Trans. Microw. Theory Tech.*, vol. 58, no. 10, pp. 2646–2653, Oct. 2010, doi: 10.1109/TMTT.2010.2065310.
- [30] N. Akozbek *et al.*, “Experimental demonstration of plasmonic Brewster angle extraordinary transmission through extreme subwavelength slit arrays in the microwave,” *Phys. Rev. B*, vol. 85, no. 20, May 2012, Art. no. 205430, doi: 10.1103/PhysRevB.85.205430.
- [31] C. Argyropoulos, G. D’Aguanno, N. Mattiucci, N. Akozbek, M. J. Bloemer, and A. Alù, “Matching and funneling light at the plasmonic Brewster angle,” *Phys. Rev. B*, vol. 85, no. 2, Jan. 2012, Art. no. 02430, doi: 10.1103/PhysRevB.85.024304.
- [32] P. Lalanne *et al.*, “Quasinormal mode solvers for resonators with dispersive materials,” *J. Opt. Soc. Am. A*, vol. 36, no. 4, pp. 686–704, 1, April, 2019, doi: 10.1364/JOSAA.36.000686.